

Multidensity integral-equation theory for short diblock hard-sphere–sticky-hard-sphere chainsNing Wu¹ and Y. C. Chiew^{2,*}¹*School of Engineering and Applied Science, Harvard University, Cambridge, Massachusetts 02138, USA*²*Department of Chemical & Biochemical Engineering, Rutgers University, Piscataway, New Jersey 08854, USA*

(Received 12 October 2009; revised manuscript received 5 March 2010; published 30 April 2010)

The multidensity Ornstein-Zernike integral equation theory is applied to study a simple model of hard sphere/sticky hard sphere diblock chains. The multidensity integral equation formalism has been successfully used to model the equilibrium structure and thermodynamic properties of homonuclear chains and shorter dimer fluids; to our knowledge it has not been applied to model diblock chains. In this work, a diblock chain fluids is represented by an m -component equal molar mixture of hard spheres with species $1, 2, \dots, m_h$ and sticky hard spheres with species m_h+1, m_h+2, \dots, m . Each spherical particle has two attractive sites A and B except species 1 and m , which have only one site per particle. In the limit of complete association, this mixture yields a system of monodisperse diblock chains. A general solution of this model is obtained in the Percus-Yevick, Polymer Percus-Yevick and ideal chain approximations. Both structural and thermodynamic properties of this model are investigated. From this study, a microphase separation is predicted for relatively short diblock symmetric and asymmetric chains. This microphase separation is enhanced at lower temperature and higher density. When chain length increases, the phase transition changes from a microphase level to a macrophase level. The size of microdomain structure is found to be dependent on total chain length, relative ratio of block lengths, temperature, and density.

DOI: [10.1103/PhysRevE.81.041809](https://doi.org/10.1103/PhysRevE.81.041809)

PACS number(s): 61.20.Gy, 61.25.he

I. INTRODUCTION

Among the different theoretical approaches in liquid state theory, the multidensity Ornstein-Zernike (MOZ) integral equation theory has proven to be a powerful method for modeling the structure, molecular correlation, and thermodynamic properties of chainlike fluids [1–6]. The MOZ theory was originally formulated to model hydrogen bonding fluids and molecules that interact through strong specific associating potentials, it has been successfully extended to model dimer fluids [7–11] and freely jointed chainlike molecules [12–19] with a variety of inter-particle pair potentials such as the hard sphere (HS) [5–7, 15–19], electrostatic [11–13], Yukawa [20, 21], and sticky hard sphere (SHS) potentials [14, 22, 23]. Most of the models studied, however, are homonuclear models in which each segment in one chain interacts with others via the same type of pair potential. A limited number of studies have examined the heteronuclear hard sphere chain models [17, 18] in which the size of each segment may be different but the type of pair potential is still the same. For complex fluids, such as polymeric chains and colloidal aggregates, the segment-segment interactions are not necessarily of the same type along the chain because of different functionality, polarity, or charges associated with different segments. Therefore, our primary interest here lies in the modeling of heteronuclear chains in which part of the segments in a chain interact with the others via a different type of pair potential than among themselves. Recent advancement of colloidal synthesis has made it possible to generate anisotropic interactions on spherical colloids, such as Janus particles [24] and patchy particles [25]. Furthermore,

controlled molecular assembly of nanoparticles, such as colloidal dimers [26], trimers [27], and chains [28], have been synthesized recently. Those “colloidal molecules” possess unique and superior capabilities to self-assemble into complex suprastructures (e.g., photonic crystals) and very rich thermodynamic behaviors have also been found in such systems [29, 30]. For example, in a model of Janus particles whose surface areas are divided into hydrophilic and hydrophobic regions, the presence of a gas-liquid critical point and micellar assembly at lower temperature were observed simultaneously [30]. We hope that the present study can inspire more experimental work on probing the phase behaviors of those “colloidal molecules.”

As a model system, in this work, we consider diblock chains that consist of a linear block of hard-sphere particles connected to a linear block of sticky-hard-sphere particles. This is an extension of our previous study of hard sphere-sticky hard sphere heteronuclear dimer fluid [14]. We show that the MOZ theory is capable of modeling the formation of microscopic domains or aggregates in the system due to the competition between repulsive and attractive interactions. The sticky hard sphere (SHS) potential model, proposed by Baxter [31], is represented by

$$\beta u(r) = \begin{cases} \infty, & 0 < r < \sigma \\ -\ln \left[\frac{d}{12\tau(d-\sigma)} \right], & \sigma < r < d, \\ 0, & r > d \end{cases} \quad (1)$$

where $\beta=1/kT$, σ represents the hard core diameter and τ^{-1} denotes the stickiness factor. In the limit of $\sigma \rightarrow d$, Eq. (1) yields an infinitely narrow and deep attractive well leading to a finite probability of finding two particles “sticking” to each other at the particle surface. Generally, τ is a monotonously increasing function of temperature and can be chosen to re-

*Author to whom correspondence should be addressed; ychiew@rci.rutgers.edu

late the potential (1) to a more realistic intermolecular potential. For example, we can choose $\tau(T)$ so that the second virial coefficient for the SHS potential, in the limit $\sigma \rightarrow d$, is the same as that of Lennard-Jones potential $u^{L-J}(r)$,

$$\int_0^\infty r^2 \{ \exp[-\beta u^{shs}(r)] - 1 \} dr = \int_0^\infty r^2 \{ \exp[-\beta u^{L-J}(r)] - 1 \} dr. \quad (2)$$

Despite its simplicity and crudeness, the study of the SHS potential is not purely an academic exercise, it has been used to study the structure of covalent liquids [32], colloidal systems [33], nonionic surfactant solutions [34], microemulsions [35], the reversible gelation and percolation [36], protein flocculation [37], and crystallization [38,39] of strongly interacting particles. The immense interests in and widespread use of the SHS model is probably because (i) the hard-core repulsion and a short-range attraction capture the essential physics of realistic interactions between particles or molecules; (ii) by varying a single parameter τ , the SHS potential can be used to model systems at different temperatures or attractive strengths, and it reduces to the hard-sphere model in the $\tau \rightarrow \infty$ limit; (iii) analytical results for the thermodynamic properties, radial distribution functions, and structure factors for particles interacting through the SHS potential are available in the Percus-Yevick (PY) approximation for one-component, multicomponent, and polydisperse mixtures; and (iv) the effect of the well depth can be isolated from the range of the potential [34].

In this work, we consider a simple linear diblock chain, consisting of two blocks of particles linked end-to-end. One of the blocks consists of a hard sphere chain, and the other is formed by a sticky hard sphere chain. The length of each block can vary from one to any positive integer. The purpose of this work is to (1) apply and generalize the multidensity integral equation theory to diblock chain architecture; (2) explore the structural properties in terms of correlation functions; (3) investigate the microphase separation phenomena which can be reflected by calculating small-angle scattering structure factors; and (4) study the thermodynamic properties via an energy route. To the best of our knowledge, the work represents a first attempt to use the multidensity integral equation theory to model diblock chain fluids.

II. MODEL

To model a monodisperse system of the HS-SHS diblock chainlike molecules, we consider a m -component equal molar mixture of species $1, \dots, i, \dots, m$, with identical diameters $R_i=1$ and number densities $\rho_i=\rho$. Species $1, 2, \dots, m_h$ are hard sphere monomers, while species m_h+1, m_h+2, \dots, m are sticky hard sphere monomers. Each monomer of species 2 to $m-1$ (except for species 1 and m) has two randomly located attraction sites, A and B on the surface. A monomer of species 1 and m , has only one attraction site on them, which are site A and B , respectively. In addition to the hard sphere and sticky hard sphere interactions, the mono-

mers interact through the associating sites A and B to form linear chainlike aggregates. In the limit of complete association, a monodisperse system of diblock HS/SHS chains (with chain length m) are formed. Each chain consists of a linear block of m_h hard sphere particles connected to a block of sticky hard sphere chain, of chain length $m_s=m-m_h$. Both m_h and m_s can be any positive integers. When $m_h=m_s$, a symmetric diblock copolymer can be modeled, and an asymmetric diblock copolymer is modeled if $m_h \neq m_s$. In the limiting case of $m_h=m_s=1$, this model becomes an HS-SHS heteronuclear dimer fluid, which was studied and reported by authors recently [14].

The pair potential $U_{ij}(12)$ among various species can be represented as

$$U_{ij}(12) = U_{ij}^{dis}(r) + U_{ij}^{ass}(12), \quad (3)$$

where $U_{ij}^{dis}(r)$ represents the dispersion interaction between particle i and j at separation r , and $U_{ij}^{ass}(12)$ is the association potential energy between species i and j , which represents the ‘‘covalent bonding’’ between two neighboring particles in a chain molecule. Indices 1 and 2 denote the positions and orientations of two interacting particles of species i and j , respectively.

The Mayer function of the dispersion potential between particle i and j , where both i and j are sticky hard spheres (i.e., $\forall i \in \{m_h+1, m_h+2, \dots, m\}$ and $\forall j \in \{m_h+1, m_h+2, \dots, m\}$), can be represented as

$$f_{ij}^{shs}(r) = \begin{cases} -1 + \frac{1}{12\tau} \delta(r-1) & 0 < r < 1 \\ 0 & r > 1 \end{cases}. \quad (4)$$

The hard sphere potential is used to represent the dispersion between particles i and j , where at least one particle is hard sphere in ij pair (i.e., either $\exists i \in \{1, 2, \dots, m_h\}$ or $\exists j \in \{1, 2, \dots, m_h\}$)

$$U_{ij}^{hs}(r) = \begin{cases} 0 & 0 < r < 1 \\ \infty & r \geq 1 \end{cases}. \quad (5)$$

The chemical association potential $U_{ij}^{ass}(12)$ can be written as

$$U_{ij}^{ass}(12) = \delta_{i+1,j} U_{AB}^{i,i+1}(12) + \delta_{i-1,j} U_{BA}^{i,i-1}(12), \quad (6)$$

where $U_{AB}^{ij}(12)$ is an infinitesimally short-ranged attractive potential between site A of species i and site B of species j , and δ_{ij} is the Kronecker delta. The orientationally averaged associative part of the Mayer function for the total potential can be represented as

$$f_{AB}^{ij}(r) = \delta_{i+1,j} f \delta(r-1), \quad (7)$$

where δ represents the Dirac delta function. The parameter f characterizes the association strength, lies between 0 and ∞ , and is related to density and the degree of association or polymerization. Our interest will focus on the complete association limit where $f \rightarrow \infty$. Readers are reminded that $f_{ij}^{shs}(r)$ and $f_{ij}^{ass}(r)$ are two distinguishable quantities even though both of them possess the Dirac delta function. The delta function in $f_{ij}^{shs}(r)$ attempts to mimic a square-well type (dispersion) interaction among species, while the delta func-

tion in $f_{ij}^{ass}(r)$ accounts for covalent bond between directly bonding species [14,22,23].

III. INTEGRAL EQUATION, IDEAL CHAIN APPROXIMATION PERCUS-YEVICK AND POLYMER PERCUS-YEVICK CLOSURE CONDITIONS

The multidensity Ornstein-Zernike formalism provides an equation relating the total and direct correlation functions $h_{\alpha\beta}^{ij}(r)$ and $c_{\alpha\beta}^{ij}(r)$. The orientationally averaged version of the multidensity Ornstein-Zernike equation, written in matrix form is given by [5,14,22,23]

$$\tilde{h}_{ij}(k) = \tilde{c}_{ij}(k) + \sum_k \tilde{c}_{ik}(k) \tilde{\sigma}^k \tilde{h}_{kj}(k). \quad (8)$$

The indices i, j , and k denote particle species which can be component 1, ..., i , ..., m . The matrix $\tilde{h}_{ij}(k)$ and $\tilde{c}_{ij}(k)$ contain the elements which are Fourier transform of the elements of the matrix $\tilde{h}_{ij}(r)$ and $\tilde{c}_{ij}(r)$. For the diblock copolymer system considered here, we have

$$\tilde{h}_{ij}(r) = \begin{pmatrix} h_{00}^{ij}(r) & h_{0A}^{ij}(r) & h_{0B}^{ij}(r) & h_{0\Gamma}^{ij}(r) \\ h_{A0}^{ij}(r) & h_{AA}^{ij}(r) & h_{AB}^{ij}(r) & h_{A\Gamma}^{ij}(r) \\ h_{B0}^{ij}(r) & h_{BA}^{ij}(r) & h_{BB}^{ij}(r) & h_{B\Gamma}^{ij}(r) \\ h_{\Gamma 0}^{ij}(r) & h_{\Gamma A}^{ij}(r) & h_{\Gamma B}^{ij}(r) & h_{\Gamma\Gamma}^{ij}(r) \end{pmatrix},$$

$$\tilde{c}_{ij}(r) = \begin{pmatrix} c_{00}^{ij}(r) & c_{0A}^{ij}(r) & c_{0B}^{ij}(r) & c_{0\Gamma}^{ij}(r) \\ c_{A0}^{ij}(r) & c_{AA}^{ij}(r) & c_{AB}^{ij}(r) & c_{A\Gamma}^{ij}(r) \\ c_{B0}^{ij}(r) & c_{BA}^{ij}(r) & c_{BB}^{ij}(r) & c_{B\Gamma}^{ij}(r) \\ c_{\Gamma 0}^{ij}(r) & c_{\Gamma A}^{ij}(r) & c_{\Gamma B}^{ij}(r) & c_{\Gamma\Gamma}^{ij}(r) \end{pmatrix},$$

$$\text{and } \tilde{\sigma}^k = \begin{bmatrix} \sigma_{\Gamma}^k & \sigma_B^k & \sigma_A^k & \sigma_0^k \\ \sigma_B^k & 0 & \sigma_0^k & 0 \\ \sigma_A^k & \sigma_0^k & 0 & 0 \\ \sigma_0^k & 0 & 0 & 0 \end{bmatrix} \quad (9)$$

The indices 0, A, B, and Γ in the correlation functions $h_{\alpha\beta}^{ij}(r)$ and $c_{\alpha\beta}^{ij}(r)$ denote the bonding states of the corresponding particles. The case of $\alpha=0$ corresponds to an unbonded particle, $\alpha=A$ or $\alpha=B$ to particle with bonded site A or B, and $\alpha=\Gamma$ to the particle with both sites bonded. The density parameters σ_{α}^k are related to the density ρ_{α}^k of α -bonded particles by

$$\sigma_0^k = \rho_0^k, \quad \sigma_A^k = \rho_0^k + \rho_A^k, \quad \sigma_B^k = \rho_0^k + \rho_B^k,$$

$$\text{and } \sigma_{\Gamma}^k = \rho_0^k + \rho_A^k + \rho_B^k + \rho_{\Gamma}^k \quad (10)$$

Equation (8) can be written in matrix form as

$$\tilde{h}(k) = \tilde{c}(k) + \tilde{c}(k) \tilde{\sigma} \tilde{h}(k). \quad (11)$$

In the above equation, $\tilde{h}(k)$ and $\tilde{c}(k)$ contain the Fourier transformed elements of $\tilde{h}(r)$ and $\tilde{c}(r)$, respectively, i.e.,

$$[\tilde{h}(r)]_{ij} = \tilde{h}_{ij}(r), \quad [\tilde{c}(r)]_{ij} = \tilde{c}_{ij}(r), \quad [\tilde{\sigma}]_{ij} = \delta_{ij} \tilde{\sigma}^i. \quad (12)$$

The PY closure for SHS-SHS interactions is given by

$$h_{\alpha\beta}^{ij}(r) = -\delta_{\alpha 0} \delta_{\beta 0} + \frac{\lambda_{\alpha\beta}^{ij}}{12} \delta(r-1) \quad 0 < r < 1, \quad (13)$$

$$c_{\alpha\beta}^{ij}(r) = -y_{\alpha\beta}^{ij}(r) + \frac{\lambda_{\alpha\beta}^{ij}}{12} \delta(r-1)$$

where $\forall i \in \{m_h+1, m_h+2, \dots, m\}$ and $\forall j \in \{m_h+1, m_h+2, \dots, m\}$ and the polymer Percus-Yevick (PPY) closure for HS-HS or HS-SHS interaction is

$$h_{\alpha\beta}^{ij}(r) = -\delta_{\alpha 0} \delta_{\beta 0} \quad 0 < r < 1, \quad (14)$$

$$c_{\alpha\beta}^{ij}(r) = -y_{\alpha\beta}^{ij}(r)$$

where at least one particle in ij pair is a hard sphere. When $r > 1$, for any pair of i and j

$$c_{\alpha\beta}^{ij}(r) = B_{\alpha\beta}^{ij} \delta(r-1), \quad (15)$$

where the constant $B_{\alpha\beta}^{ij}$ is related to the association strength f and contact values of the cavity functions $y_{\alpha\beta}^{ij}(r)$ by

$$B_{AB}^{ij} = \delta_{j,i+1} y_{00}^{ij}(1^+) f, \quad B_{BA}^{ij} = \delta_{j,i-1} y_{00}^{ij}(1^+) f,$$

$$B_{A\Gamma}^{ij} = \delta_{j,i+1} y_{0A}^{ij}(1^+) f, \quad B_{\Gamma A}^{ij} = \delta_{j,i-1} y_{0A}^{ij}(1^+) f,$$

$$B_{B\Gamma}^{ij} = \delta_{j,i-1} y_{0B}^{ij}(1^+) f, \quad B_{\Gamma B}^{ij} = \delta_{j,i+1} y_{0B}^{ij}(1^+) f,$$

$$B_{\Gamma\Gamma}^{ij} = \delta_{j,i-1} y_{AB}^{ij}(1^+) f + \delta_{j,i+1} y_{BA}^{ij}(1^+) f,$$

$$B_{0\alpha}^{ij} = B_{\alpha 0}^{ij} = 0 \quad (\alpha \in \{0, A, B, \Gamma\}), \quad B_{AA}^{ij} = B_{BB}^{ij} = 0. \quad (16)$$

In Eq. (13), the quantity $\lambda_{\alpha\beta}^{ij}$ is an as yet unknown dimensionless parameter and can be related to τ by

$$\tau \lambda_{\alpha\beta}^{ij} = y_{\alpha\beta}^{ij}(1). \quad (17)$$

The densities ρ_{α}^i can be determined by the self-consistent relations,

$$c_A^i = 24f [y_{00}^{i,i+1}(1^+) \eta_A^{i+1} + y_{0A}^{i,i+1}(1^+) \eta_0^{i+1}], \quad (18a)$$

$$c_B^i = 24f [y_{00}^{i,i-1}(1^+) \eta_B^{i-1} + y_{0B}^{i,i-1}(1^+) \eta_0^{i-1}], \quad (18b)$$

$$c_{\Gamma}^i = 24f [y_{B0}^{i,i+1}(1^+) \eta_A^{i+1} + y_{BA}^{i,i+1}(1^+) \eta_0^{i+1}]$$

$$= 24f [y_{A0}^{i,i-1}(1^+) \eta_B^{i-1} + y_{AB}^{i,i-1}(1^+) \eta_0^{i-1}], \quad (18c)$$

where the correlation functions of the first hierarchy c_{α}^i are related to the density parameters by

$$c_A^i = \frac{\sigma_A^i}{\sigma_0^i} - 1 \quad c_B^i = \frac{\sigma_B^i}{\sigma_0^i} - 1 \quad c_{\Gamma}^i = \frac{\sigma_{\Gamma}^i}{\sigma_0^i} - \frac{\sigma_A^i \sigma_B^i}{(\sigma_0^i)^2} \quad (19)$$

and $\eta_{\alpha}^i = \frac{\pi}{6} \sigma_{\alpha}^i R_i^3$.

In the present work, we obtain the solution to the multidensity integral equation in the ideal chain approximation, which has been applied to the study of homonuclear [5,6] and heteronuclear [40] chain fluids. In the ideal chain approximation, some graphs that account for the effect of hard core repulsions on the intramolecular correlations are ne-

neglected so that the intramolecular correlations for $x > 1$ are those of “ideal” chains. The nonoverlap between intramolecular monomers is, however, retained through the hard-core repulsion ($x < 1$). This approximation has been widely utilized in thermodynamic perturbation theory (TPT) for the polymeric systems [3,4], as well as integral equation theory for linear hard sphere chains [5]. Theoretical predictions based on this approximation agree with computer simulations very well. Mathematically speaking, all the particle correlation functions $h_{\alpha\beta}^{ij}(r)$, $c_{\alpha\beta}^{ij}(r)$, and constants $B_{\alpha\beta}^{ij}$ with either $\alpha = \Gamma$ or $\beta = \Gamma$ are set to zero, i.e.,

$$B_{\alpha\Gamma}^{ij} = B_{\Gamma\alpha}^{ij} = 0 \quad \text{for } \alpha \in \{0, A, B, \Gamma\}. \quad (20)$$

Under these conditions, the fourth row and column of the original matrixes in Eq. (9) are neglected so that $\tilde{h}_{ij}(k)$, $\tilde{c}_{ij}(k)$ and $\tilde{\sigma}^k$ becomes 3×3 matrixes.

IV. GENERAL SOLUTIONS OF THE MODELS

To solve Eq. (11) for the correlation functions, we use Baxter’s factorization method to de-couple the functions $\tilde{h}(k)$ and $\tilde{c}(k)$ through the introduction of the so-called $\tilde{q}(k)$ function to obtain

$$rc_{\alpha\beta}^{ij}(r) = -[q_{\alpha\beta}^{ij}(r)]' + 2\pi \sum_k \sum_{\gamma\delta} \frac{\partial}{\partial r} \left(\int_0^{1-r} q_{\gamma\alpha}^{ki}(t) \times \sigma_{\gamma\delta}^k q_{\delta\beta}^{kj}(r+t) dt \right) \quad 0 < r < 1, \quad (21)$$

$$rh_{\alpha\beta}^{ij}(r) = -[q_{\alpha\beta}^{ij}(r)]' + 2\pi \sum_k \sum_{\gamma\delta} \int_0^1 q_{\alpha\gamma}^{ik}(t) \sigma_{\gamma\delta}^k \times h_{\delta\beta}^{kj}(|r-t|)(r-t) dt \quad r > 0. \quad (22)$$

The function $q_{ij}^{\alpha\beta}(r)$ is short-ranged and vanishes for $r < 0$ and $r > 1$.

In the complete association limit ($f \rightarrow \infty$), we combine the self-consistent relations Eq. (18) and (19) and the ideal chain approximation Eq. (20) to obtain

$$\tilde{B}_{AB}^{i,i+1} = \frac{m}{24\eta} (1 - \delta_{i,m}), \quad (23)$$

where η refers to the packing fraction of segments, i.e., $\eta = \frac{\pi}{6} R^3 m \rho$ and $\tilde{B}_{\alpha\beta}^{ij} = \frac{\eta_{1-\alpha} \eta_{1-\beta}}{\eta_i \eta_j} B_{\alpha\beta}^{ij}$

For the sake of simplicity, Eq. (22) can be written as

$$r\tilde{h}_{\alpha\beta}^{ij}(r) = -\tilde{q}_{\alpha\beta}^{ij}(r) + 12 \frac{\eta}{m} \sum_k \sum_{\gamma\delta} \int_0^1 \tilde{q}_{\alpha\gamma}^{ik}(t) \times \tilde{h}_{\delta\beta}^{kj}(|r-t|)(r-t) Z_{\gamma\delta}^k dt \quad r > 0, \quad (24)$$

where $\tilde{h}_{\alpha\beta}^{ij} = \frac{\eta_{1-\alpha} \eta_{1-\beta}}{\eta_i \eta_j} h_{\alpha\beta}^{ij}$, $\tilde{q}_{\alpha\beta}^{ij} = \frac{\eta_{1-\alpha} \eta_{1-\beta}}{\eta_i \eta_j} q_{\alpha\beta}^{ij}$, and $Z_{\alpha\beta}^i = 1$ except $Z_{AA}^i = Z_{BB}^i = 0$.

Consider Eq. (24) in the range of $0 < r < 1$, we obtain a second order polynomial for the q functions. We will not reproduce the detailed mathematical derivation and solution

since they are similar to the earlier models studied by the authors [14,22,23]. The resulting equations are shown below.

If both $\forall i \in \{m_h + 1, m_h + 2, \dots, m\}$ and $\forall j \in \{m_h + 1, m_h + 2, \dots, m\}$,

$$\tilde{q}_{\alpha\beta}^{ij}(r) = \delta_{\beta 0} \left[\frac{1}{2} \tilde{a}_{\alpha}^i (r^2 - 1) + \tilde{b}_{\alpha}^i (r - 1) \right] + \tilde{\lambda}_{\alpha\beta}^{ij} + \tilde{B}_{\alpha\beta}^{ij}; \quad (25)$$

If either $\exists i \in \{1, 2, \dots, m_h\}$ or $\exists j \in \{1, 2, \dots, m_h\}$,

$$\tilde{q}_{\alpha\beta}^{ij}(r) = \delta_{\beta 0} \left[\frac{1}{2} \tilde{a}_{\alpha}^i (r^2 - 1) + \tilde{b}_{\alpha}^i (r - 1) \right] + \tilde{B}_{\alpha\beta}^{ij}. \quad (26)$$

The coefficients of the q functions are summarized in the Appendix. Once $\tilde{q}_{\alpha\beta}^{ij}(r)$ is known, the explicit expressions for the contact value of correlation function $\tilde{g}_{\alpha\beta}^{ij}(1^+)$ can be evaluated from Eq. (22) and they are summarized in the Appendix too.

In general, the parameters $\tilde{\lambda}_{\alpha\beta}^{ij}$ in Eqs. (A6) are functions of particle packing fraction η , temperature τ , total chain length m , length of sticky hard sphere block m_s (or length of hard sphere block m_h) and association strength f . In the complete association limit, $\tilde{\lambda}_{\alpha\beta}^{ij}$ will be a function of η , m , m_s (or m_h) and τ only. Therefore, in order to obtain $\tilde{\lambda}_{\alpha\beta}^{ij}$, we have to solve a set $6m_s^2$ of nonlinear algebraic equations [Eqs. (A6)], including some trivial equations, for example $\tilde{\lambda}_{AB}^{mj}$ for the ending segments. Correct zero-density limit of $\tilde{\lambda}_{ij}^{\alpha\beta}$ must be taken to avoid unphysical solutions [14,22,23]. Unfortunately we are unable to find the analytical solution of $\tilde{\lambda}_{ij}^{\alpha\beta}$ at zero-density limit due to the nonlinear nature of the resulting algebraic equations. Hence, we propose that $\tilde{\lambda}_{\alpha\beta}^{ij} = 0$ except $\tilde{\lambda}_{00}^{ij} = \frac{1}{12\tau}$ and $\eta \tilde{\lambda}_{AB}^{ij} = 0$ are used as an input (corresponding to sticky hard sphere monomers) in the modified Newton’s method for solving $6m_s^2$ nonlinear algebraic equations mentioned above in the zero-density limit. As in the case of sticky hard sphere chain [23], when $\eta \rightarrow 0$, $\tilde{\lambda}_{AB}^{ij}$, $\tilde{B}_{AB}^{i,i+1}$, and $\tilde{B}_{BA}^{i,i-1}$ increases without limit. One can multiply η at both sides of Eq. (A6f) and solve for $\tilde{\lambda}_{00}^{ij}$, $\tilde{\lambda}_{A0}^{ij}$, $\tilde{\lambda}_{B0}^{ij}$, $\tilde{\lambda}_{AA}^{ij}$, $\tilde{\lambda}_{BB}^{ij}$, $\eta \tilde{\lambda}_{AB}^{ij}$ simultaneously. When τ increases, the potential of $U_{ij}^{shs}(r)$ approaches that of hard sphere. When $\tau \rightarrow \infty$, $\tilde{\lambda}_{\alpha\beta}^{ij}$ becomes zero (for nonzero density), we can recover the solutions of hard sphere chains.

The segment-segment pair correlation function $h_{ij}(r)$ is defined as

$$h_{ij}(r) = \sum_{\alpha} \sum_{\beta} \tilde{h}_{\alpha\beta}^{ij}(r), \quad (27)$$

where the summation runs over all bonding state.

The segment-segment and segment-averaged radial distribution function (RDF) for a monodisperse system is defined as

$$g_{ij}(r) = 1 + h_{ij}(r) \quad (28)$$

and

$$g(r) = \frac{1}{m^2} \sum_i \sum_j g_{ij}(r). \quad (29)$$

For $r > 1$, the correlation functions of a diblock chain can be calculated from Eq. (22) and summarized as

For $j \in \{1, 2, \dots, m_h\}$

$$\begin{aligned} r\tilde{h}_{\alpha\beta}^{ij}(r) &= \frac{12\eta}{m} \sum_{k=1}^m \sum_{\gamma\delta} \int_0^1 \tilde{q}_{\alpha\gamma}^{ik}(t)(r-t)\tilde{h}_{\delta\beta}^{kj}(r-t)Z_{\gamma\delta}^k dt \\ &+ \frac{12\eta}{m} \sum_{k=1}^m \sum_{\gamma\delta} \tilde{q}_{\alpha\gamma}^{ik}(r-1)\tilde{B}_{\delta\beta}^{kj}Z_{\gamma\delta}^k. \end{aligned} \quad (30a)$$

For $j \in \{m_h+1, m_h+2, \dots, m\}$

$$\begin{aligned} r\tilde{h}_{\alpha\beta}^{ij}(r) &= \frac{12\eta}{m} \sum_{k=1}^m \sum_{\gamma\delta} \int_0^1 \tilde{q}_{\alpha\gamma}^{ik}(t)(r-t)\tilde{h}_{\delta\beta}^{kj}(r-t)Z_{\gamma\delta}^k dt \\ &+ \frac{12\eta}{m} \sum_{k=1}^m \sum_{\gamma\delta} \tilde{q}_{\alpha\gamma}^{ik}(r-1)\tilde{B}_{\delta\beta}^{kj}Z_{\gamma\delta}^k \\ &+ \frac{12\eta}{m} \sum_{k=m_h+1}^m \sum_{\gamma\delta} \tilde{q}_{\alpha\gamma}^{ik}(r-1)\tilde{\lambda}_{\delta\beta}^{kj}Z_{\gamma\delta}^k. \end{aligned} \quad (30b)$$

The second term on the right-hand side of Eq. (30a) and (30b) come from the explicit treatment of the association delta functions of $h_{\alpha\beta}^{ij}(r)$ at contact while the last term in Eq. (30b) comes from the explicit treatment of the dispersion delta functions of $h_{\alpha\beta}^{ij}(r)$ at contact.

V. RESULTS AND DISCUSSION

A. Distribution functions

By using $\tilde{g}_{\alpha\beta}^{ij}(1^+)$ in Eqs. (A4)–(A6) as initial values, the distribution functions $\tilde{g}_{\alpha\beta}^{ij}(r)$ of a diblock chains beyond the hard core region can be calculated using Perram's iteration method [41]. Besides the overall radial distribution function defined in Eq. (29), we are also interested in the partial averaged radial distribution functions (RDF) defined by

$$\begin{aligned} g_{hh}(r) &= \frac{1}{m_h^2} \sum_{i=1}^{m_h} \sum_{j=1}^{m_h} g_{ij}(r), \\ g_{ss}(r) &= \frac{1}{m_s^2} \sum_{i=m_h+1}^m \sum_{j=m_h+1}^m g_{ij}(r), \text{ and} \\ g_{hs}(r) &= \frac{1}{m_h m_s} \sum_{i=1}^{m_h} \sum_{j=m_h+1}^m g_{ij}(r). \end{aligned} \quad (31)$$

They are related to the overall RDF by

$$g(r) = \rho_h \rho_h g_{hh}(r) + \rho_s \rho_s g_{ss}(r) + 2\rho_h \rho_s g_{hs}(r), \quad (32)$$

where $\rho_h = m_h/m$ and $\rho_s = m_s/m$.

The curves shown in Figs. 1 and 2 are the partial RDFs for completely associated symmetric diblock chains with different chain lengths ($m_s = m_h = 3$ and $m_s = m_h = 2$, respectively) at different densities. At low densities, $g_{hh}(1^+)$ is less than unity and this is partially due to exclusion of monomers from

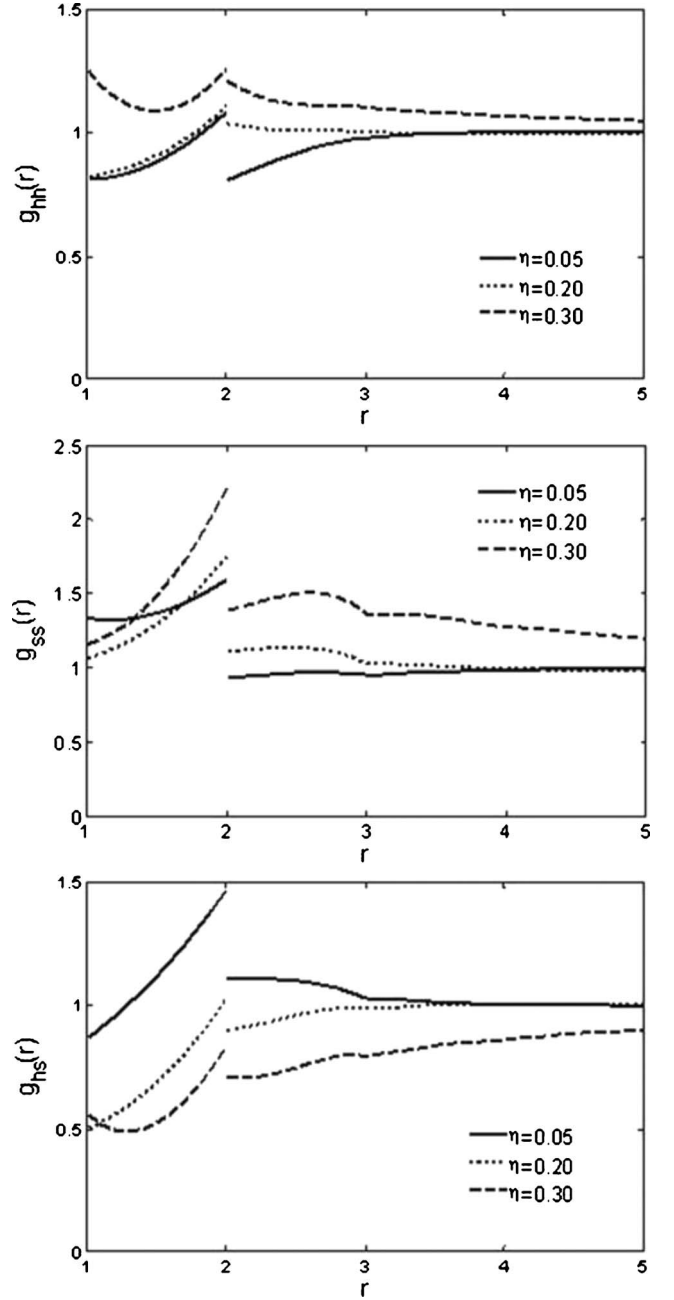


FIG. 1. The partial radial distribution functions for a symmetric diblock hexamer ($m_s = m_h = 3$) at different densities with a stickiness parameter of $\tau = 0.15$.

close approach in different chains. Low values of $g_{hs}(1^+)$ especially at high densities indicate the formation of clusters. The appearance of cusp or discontinuity in the function $g_{hh}(r)$ at $r=2$ is due to the presence of intramolecular rigidity constraints (hard core) between chain segments. For hexamer, the most significant source of intramolecular correlations is from two particles separated by two bonds which induces the discontinuity at $r=2$. The function $g_{hh}(r)$ is continuous (but with cusp) for a tetramer at $r=2$ because the only intramolecular correlation for hard spheres comes from two directly bonded spheres for $r < 1$; this correlation effect is absent when $r > 1$. Since the intermolecular correlations

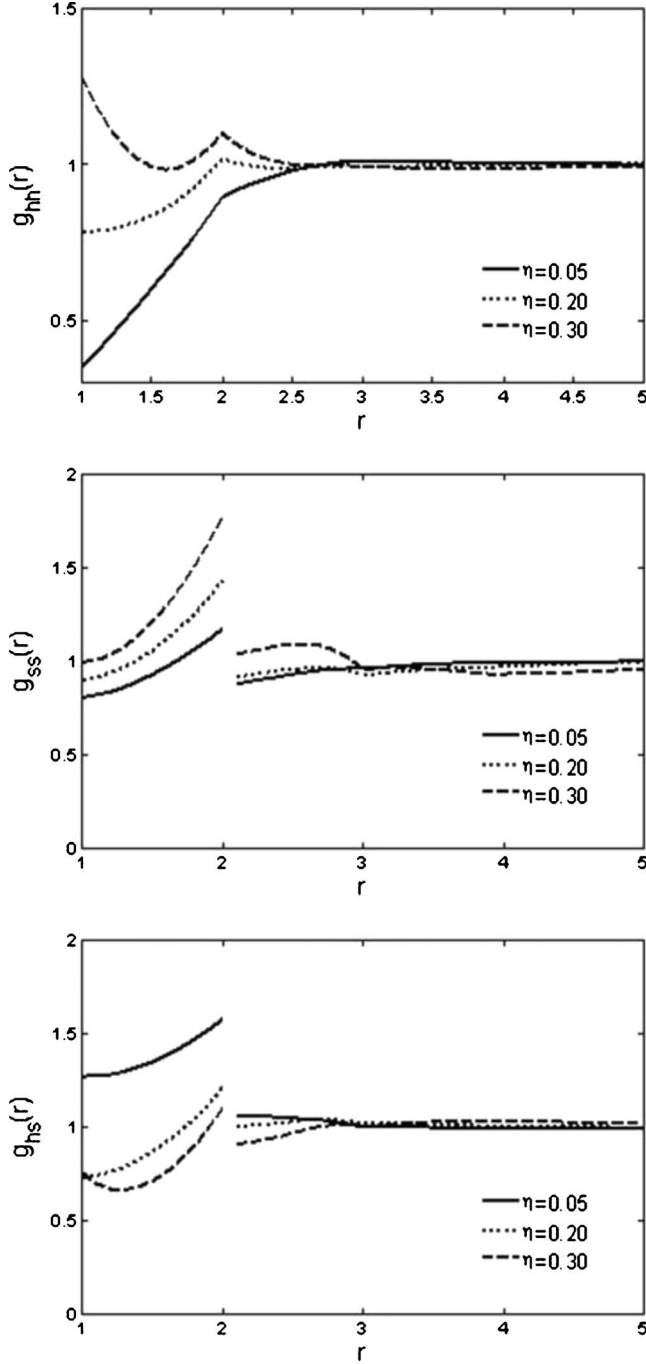


FIG. 2. The partial radial distribution functions for a symmetric diblock tetramer ($m_s=m_h=2$) at different densities with a stickiness parameter of $\tau=0.12$.

are expected to be dominant at high densities, the magnitude of jump in $g_{hh}(r)$ decreases with increasing densities. On the other hand, discontinuity (but no cusp) is also seen in $g_{ss}(r)$ at $r=2$ although its origin is different from that of $g_{hh}(r)$. Mathematically, the discontinuity in $g_{ss}(r)$ arises from the last two terms in Eq. (30b). Physically, it can be seen that besides the intramolecular correlations that induces discontinuity in $g_{hh}(r)$ at $r=2$, the intermolecular correlation can also induce discontinuity in $g_{ss}(r)$. That intermolecular correlation is the interaction between two sticky hard spheres from dif-

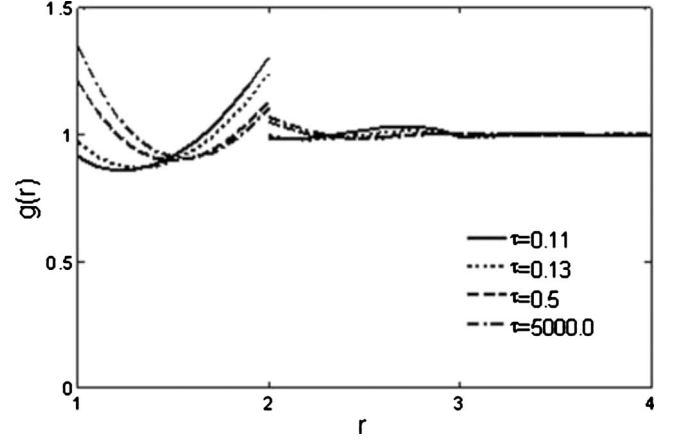


FIG. 3. The overall distribution function for a symmetric diblock tetramer ($m_s=m_h=2$) at different temperatures with a constant density of $\eta=0.30$.

ferent chains but separated with *one* sticky hard sphere adhering to either one of those two particles or to both of them. Thus, the magnitude of jump in $g_{ss}(r)$ at $r=2$ increases as density increases, and the similar trend is also observed in our previous studies on sticky hard-sphere chain fluids [23]. Since the interaction between hard sphere and sticky hard-sphere is of the hard sphere type, it is not surprising to see the magnitude of jump in $g_{hs}(r)$ at $r=2$ shows a trend similar to that of $g_{hh}(r)$.

The overall distribution function for a symmetric diblock tetramer ($m_h=m_s=2$) at different temperatures is plotted in Fig. 3. The function $g(r)$ approaches unity faster at higher temperature. The contact value of $g(r)$ increases with increasing temperature and the magnitude of jump at $r=2$ decreases as temperature increases since at higher temperature the sticky strength is weaker. When $\tau \rightarrow \infty$, we recover the results for homonuclear hard sphere chain fluids.

B. Structure factors

Static structure factor can give important information on the formation of microstructures within the bulk fluid and it is one of our primary foci in this work. Experimentally, the structure factors can be probed through the small angle neutron scattering (SANS) or the small angle x-ray scattering spectra, from which information on microscopic structures and interaction potentials can be inferred. Theoretically, the structure factor $S(k)$ can be obtained from a Fourier transform of $g(r)$,

$$S(k) = 1 + 4\pi\rho \int_0^\infty [g(r) - 1]r^2 \frac{\sin kr}{kr} dr. \tag{33}$$

For our specific system of diblock chains, we have

$$S(k) = 1 + \frac{2(m-1) \sin k}{m k} + 24\eta \left[\frac{1}{m^2} \sum_{i=m_h+1}^m \sum_{j=m_h+1}^m \sum_{\alpha} \sum_{\beta} \tilde{\chi}_{\alpha\beta}^{ij} \frac{\sin k}{k} \right] + 24\eta \int_0^\infty [g(r) - 1]r \frac{\sin kr}{k} dr. \tag{34}$$

The first three terms on the right hand side of Eq. (34) follow from the Fourier transform of the δ -functions that account for the self-correlation, the nearest-neighbor bonding (with the ideal chain approximation incorporated) and the nearest-neighbor non-bonding contributions, respectively. The last term on the right-hand side of Eq. (34) accounts for the contribution from the regular part of $g(r)$. The structure factor $S(k)$ is related to the partial structure factors by $S(k) = \sum_i \sum_j S_{ij}(k)$ where the partial structure factors $S_{ij}(k)$ is defined as

$$S_{ij}(k) = x_i \delta_{ij} + x_i x_j 4\pi\rho \int_0^\infty \left[\sum_\alpha \sum_\beta \tilde{g}_{\alpha\beta}^{ij}(r) - 1 \right] r^2 \frac{\sin kr}{kr} dr. \quad (35)$$

Here, x_i is the number concentration of species i and $x_i = \rho_i / \rho = 1/m$.

We investigate three partial structure factors: $S_{hh}(k)$ for hard-hard spheres, $S_{ss}(k)$ for sticky-sticky hard spheres, and $S_{hs}(k)$ for hard-sticky hard spheres. They are defined as

$$\begin{aligned} S_{hh}(k) &= \sum_{i=1}^{m_h} \sum_{j=1}^{m_h} S_{ij}(k), \\ S_{ss}(k) &= \sum_{i=m_h+1}^m \sum_{j=m_h+1}^m S_{ij}(k), \\ S_{hs}(k) &= \sum_{i=1}^{m_h} \sum_{j=m_h+1}^m S_{ij}(k) = \sum_{i=m_h+1}^m \sum_{j=1}^{m_h} S_{ij}(k). \end{aligned} \quad (36)$$

It is convenient to work with the partial structure factors normalized by the block group concentrations defined as

$$\begin{aligned} S_{hh}(k)/\rho_h &= 1 + \frac{2(m_h - 1) \sin k}{m_h k} \\ &\quad + 24\eta\rho_h \int_0^\infty [g_{hh}(r) - 1] r^2 \frac{\sin kr}{kr} dr, \\ S_{ss}(k)/\rho_s &= 1 + \frac{2(m_s - 1) \sin k}{m_s k} \\ &\quad + 24 \frac{\eta}{\rho_s} \left[\frac{1}{m^2} \sum_{i=m_h+1}^m \sum_{j=m_h+1}^m \sum_\alpha \sum_\beta \tilde{\chi}_{\alpha\beta}^{ij} \frac{\sin k}{k} \right] \\ &\quad + 24\eta\rho_s \int_0^\infty [g_{ss}(r) - 1] r^2 \frac{\sin kr}{kr} dr, \\ S_{hs}(k)/\sqrt{\rho_h \rho_s} &= \frac{1}{m^2 \sqrt{\rho_h \rho_s}} \frac{\sin k}{k} \\ &\quad + 24\eta\sqrt{\rho_h \rho_s} \int_0^\infty [g_{hs}(r) - 1] r^2 \frac{\sin kr}{kr} dr. \end{aligned} \quad (37)$$

In Figs. 4(a) and 4(b), we present the total and partial structure factors at low and wide-angle regimes for a sym-

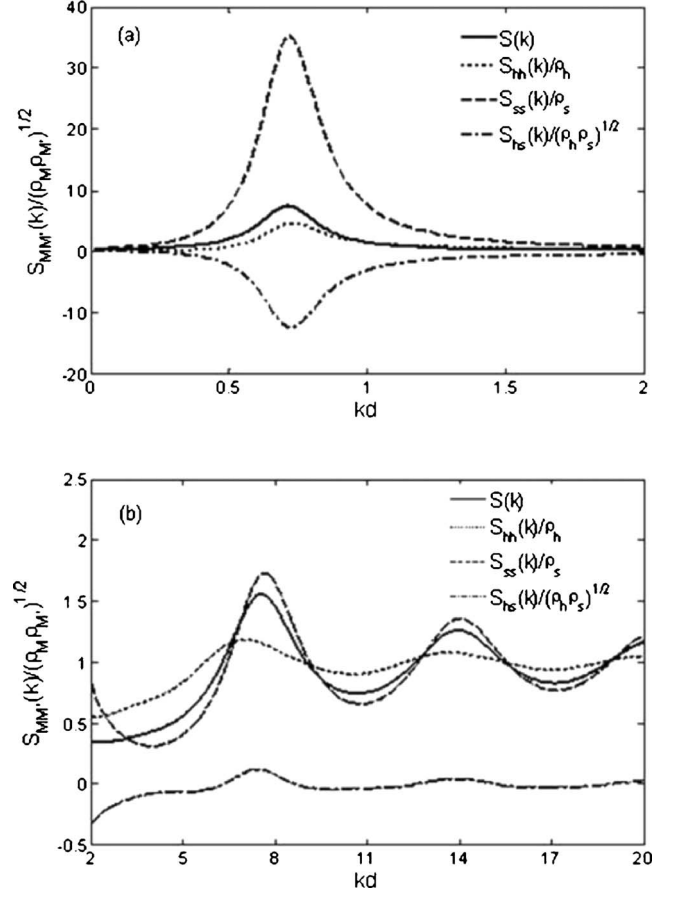


FIG. 4. The total and partial structure factors for a symmetric diblock tetramer at stickiness parameter of $\tau=0.10$ and density of $\eta=0.30$ in the low-angle regime (a) and the wide-angle regime (b).

metric diblock tetramer ($m_h=2, m_s=2$) at stickiness parameter of $\tau=0.10$ and density of $\eta=0.30$. A sharp low-angle peak emerges around $k^*=0.72/d$ for $S_{ss}(k)$. It is strong enough to generate a peak at the same position in the total structure factor $S(k)$. This peak is generally thought to be an “order parameter” and clearly indicates a formation of aggregates or microdomain structures due to the strong attractive interaction among sticky hard spheres. The peak position k^* corresponds to the periodic spacing between microdomains and can be determined as $D=2\pi/k^* \approx 8.7d$, which is much longer than the full chain length of $l=4d$. The negative sign of the small-angle peak in $S_{hs}(k)$ implies that an excess (or a lack) in hard sphere monomers is spatially correlated with a lack (or an excess) of sticky hard sphere monomers. From Fig. 4(b), it can be seen that although the height of wide-angle peak in $S_{ss}(k)$ is much smaller than that of low-angle peak, it is still the dominant component in the total scattering intensity profile.

The degree of order for a microdomain structure can be characterized by the maximum intensity of the small-angle scattering. It is expected that the order of microdomain structure increases with decreasing temperatures at a constant density since the association strength of sticky hard spheres is larger at lower temperature. This tendency is shown in Fig. 5(a) where $S_{ss}(k)$ is plotted as a function of temperatures. When temperature τ decreases, the low-angle peak increases

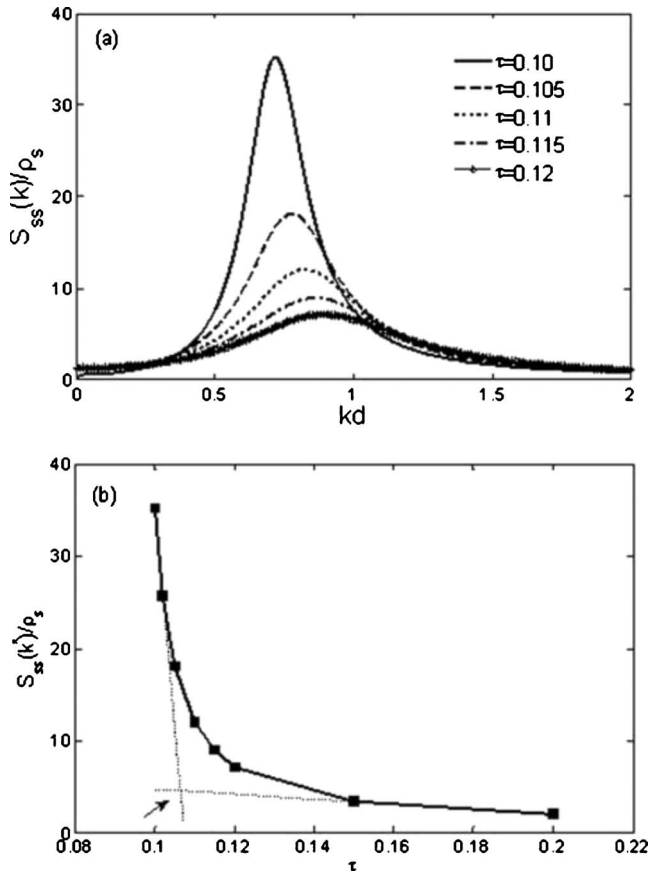


FIG. 5. Structure factors for the sticky hard spheres in a symmetric diblock tetramer at different temperatures ($\eta=0.30$). (a) the scattering profile; (b) the maximum intensity of low-angle peak.

dramatically and becomes sharper. On the other hand, no low-angle peak can be observed at sufficiently high temperature and the profile of $S_{ss}(k)$ approaches that of $S_{hh}(k)$ as $\tau \rightarrow \infty$. Also we can see a shift of that peak to smaller wave vectors which correspond to larger microdomain structures. The wide-angle scattering profiles, which are not shown here, are found to be essentially the same at different temperatures. We are not able to find an analytical expression for the “transition temperature τ_1 ” that corresponds to the emergence of the low angle peak, i.e., the onset of microdomain formation. This temperature τ_1 , however, can be estimated from Fig. 5(b) by plotting the peak intensity vs. temperature. Similarly, at a constant temperature there exists a “transition density” beyond which microdomain formation becomes significant, as shown in Fig. 6. Again, the shift of the peak position to lower wave numbers indicates formation of larger clusters. The rapidly growing peak intensity with decreasing temperature suggests the existence of a second “transition temperature τ_2 ” below which nonzero k peak diverges. In fact, one can plot $1/S(k^*)$ as a function of τ and extrapolate the temperature where $1/S(k^*)$ approaches zero. τ_2 is ~ 0.095 for symmetric tetramer at density $\eta=0.3$. Unlike the common fluid-fluid phase transition, a fluid-clustered/ordered phase transition, or equivalently a “microphase separation” occurs below this transition temperature.

The multidensity integral equation does not provide additional structure information other than what we reported.

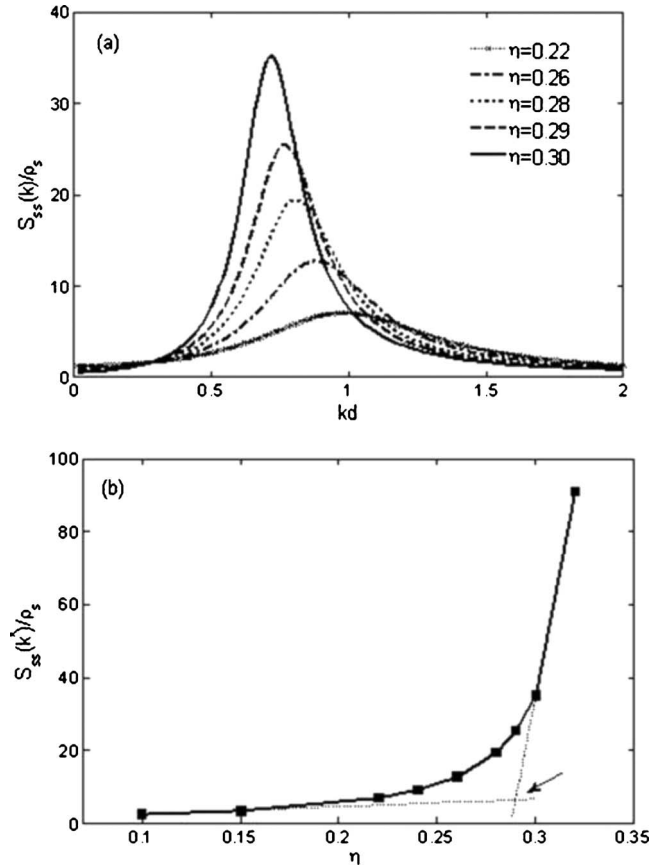


FIG. 6. Structure factors for the sticky hard spheres in a symmetric diblock tetramer at different densities ($\tau=0.10$). (a) the scattering profile; (b) the maximum intensity of low-angle peak.

Hence it is not possible to interpret the microdomain structure without some level of speculation. For example, in Figs. 4 and 5, the domain spacing $D \sim 8.7d$, larger than the full chain length is interesting. One speculative structure may be that the clusters are separated far from each other and the space between them filled with nonassociated chains without any preferred orientation or association. Other structures are also possible. Unfortunately the integral equation approach cannot provide unequivocal interpretation of the microdomain structure. The theory does predict the occurrence of microphase separation and indicate how it is affected by density, temperature, and chain architecture (see below). To gain more detailed information, molecular simulation can be used to elucidate the microdomain structure predicted by the theory.

We also study the structure factors of longer diblock chains, such as an asymmetric diblock octamer ($m_h=2$ and $m_s=6$) shown in Fig. 7. At high temperature, the association strength is too weak to induce microdomain formation. As temperature decreases, microdomains start to emerge as a peak at nonzero wave numbers shows up. At sufficiently low temperature, the peak does not diverge at a nonzero k . Instead, a peak emerges at $k=0$ and $S_{ss}(k=0)$ exceeds 100 at $\tau=0.14$. The disappearance of microdomains indicates that the attraction is too strong to maintain a finite size cluster structure, so system approaches a spinodal for common fluid-fluid phase transition. Therefore, one can observe a

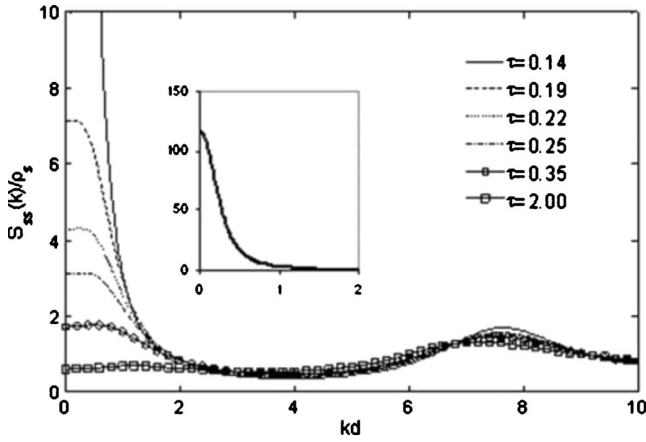


FIG. 7. Structure factors for the sticky hard spheres in an asymmetric diblock octamer ($m_h=2$ and $m_s=6$) at different temperatures ($\eta=0.3$). The inset shows that a peak emerges at zero wave number when τ is 0.14.

microdomain formation only within an intermediate temperature range (or association strength) due to a delicate balance between repulsive and attractive interactions within the fluid.

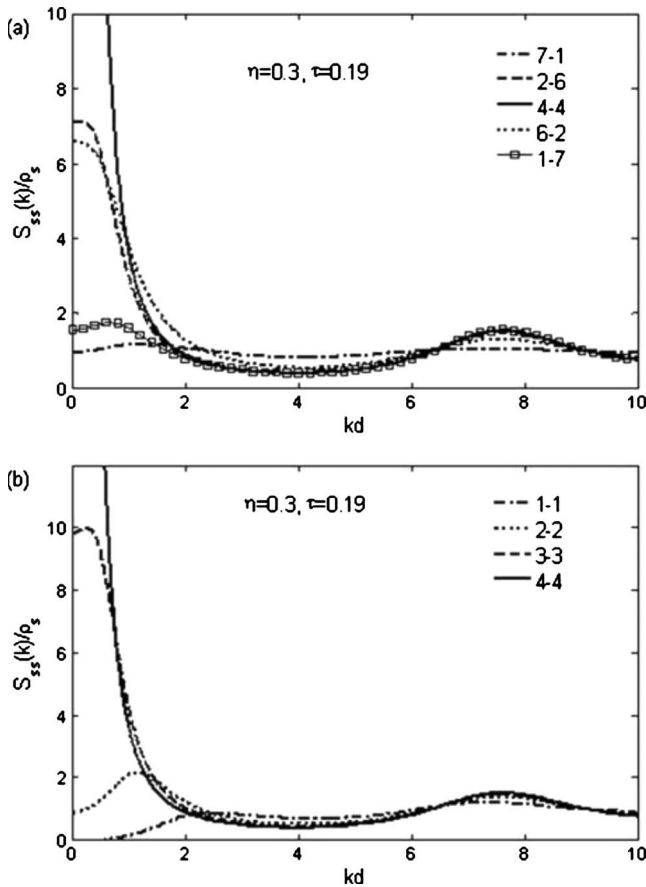


FIG. 8. Structure factors for the sticky hard spheres for a series of diblock HS-SHS chains. (a) Octamers with different lengths of hard sphere blocks. (b) Symmetric chains with different lengths. Chains are labeled as m_H-m_S . For example, “6–2” indicates an octamer with six hard spheres and two sticky hard spheres.

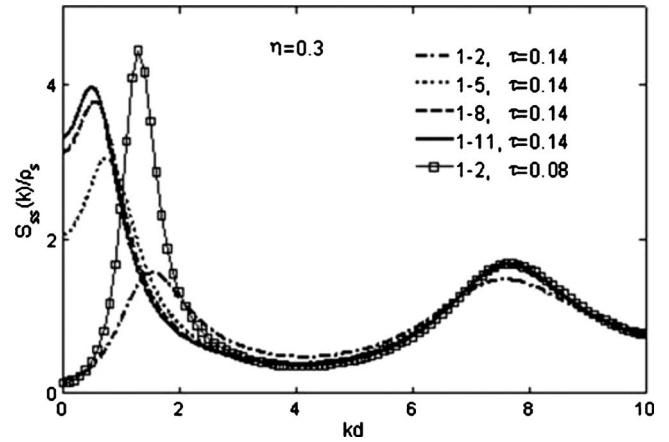


FIG. 9. Structure factors for the sticky hard spheres in asymmetric surfactantlike chains of different lengths. Different chains are labeled as $1-m_s$. For example, “1–5” indicates a hexamer with one hard sphere and five sticky hard spheres.

In addition to temperature effect, the architecture and chain length have impacts on microdomain formation too. Shown in Fig. 8(a), peaks at nonzero wave numbers emerge for asymmetric octamers, while at the same temperature the symmetric one shows a peak at $k=0$. For symmetric diblock chains with the same monomer-monomer attractive strength, longer chains tend to form larger and irregular clusters. Therefore, the peaks in Fig. 8(b) shift to smaller wave numbers (until $k=0$) as chain length increases.

We now turn to extremely asymmetric diblock chains, i.e., the block of sticky hard spheres varies its length but the number of hard spheres is fixed at *one*. This could be a primitive representation of surfactantlike molecules in which short head groups repulse each other and longer tails interact via hydrophobic attractions. Figure 9 shows the formation of microdomains for different chain lengths ($1-m_s$) at the same density and temperature, indicated by the emergence of the low-angle peak. The peak position shifts to smaller wave numbers because the size of clusters increases as chains become longer. $S_{ss}(k=0)$ increases as surfactant becomes longer. This indicates that the phase transition may change from a microphase level to a macrophase level as chain length increases. This shift to zero wave vector is not surprising since for $m_s \gg 1$, the chain is expected to behave as pure sticky hard sphere chains which we have shown to exhibit macrophase separation [23]. Stronger attraction is required to form ordered domains for shorter chains. Therefore, the peak intensity of 1–2 chain is comparable to longer chains at much lower temperature, as shown in the inset of Fig. 9. If we compare the asymmetric chain 1–3 chain to the symmetric tetramer 2–2 the same density ($\eta=0.30$) and temperature ($\tau=0.10$), we find that the microdomain spacing in the asymmetric system ($\approx 6.7d$) is smaller than that of the diblock cotetramer ($\approx 8.7d$). This is probably because stronger SHS attractive interaction exists among the asymmetric chains resulting in more compact aggregates.

C. Thermodynamic properties

The equation of state is calculated via a standard energy route which we developed before [14,22,23]. The HS-SHS

block copolymer model we consider here consists of an equal molar mixture of m_h -component hard-spheres of species $1, \dots, i, \dots, m_h$ and m_s -component sticky hard-spheres of species m_h+1, m_h+2, \dots, m which have identical stickiness. The total number of particles is $N = \sum_{i=1}^m N_i$, where N_i is the number of particles for species i . The Helmholtz energy A can be written as (with density independent terms omitted),

$$\beta A = -\ln Z_N = -\ln \int e^{-\beta U_N(r_1, r_2, \dots, r_N)} dr_1 dr_2 \dots dr_N, \quad (38)$$

where $\beta = 1/kT$

Differentiating Eq. (44) with respect to τ gives

$$\frac{\partial(\beta A)}{\partial \tau} = -\frac{1}{Z} \int \frac{\partial[-\beta U_N(r^N)]}{\partial \tau} e^{-\beta U_N(r^N)} dr^N. \quad (39)$$

Notice that

$$\beta U_{ij}(r) = \begin{cases} \beta U_{ij}^{shs}(r) + \beta U_{ij}^{ass}(r) & \text{for } i \wedge j \in \{m_h+1, m_h+2, \dots, m\} \\ \beta U_{ij}^{hs}(r) + \beta U_{ij}^{ass}(r) & \text{for } i \vee j \in \{1, 2, \dots, m_h\} \end{cases}$$

is the interaction between species i and j . If we consider both the chemical association and the hard-sphere potential are independent of temperature, then

$$\frac{\partial[\beta U_{ij}(r)]}{\partial \tau} = \frac{1}{\tau} \quad \text{if } d^- < r < d, \text{ and zero elsewhere.} \quad (43)$$

Substituting Eq. (43) into Eq. (42), we can obtain

$$\frac{\partial(\beta A/N_C)}{\partial \tau} = 2\pi\rho_C \sum_{i=m_h+1}^m \sum_{j=m_h+1}^m \int_{d^-}^d \tau^{-1} g_{ij}(r) r^2 dr. \quad (44)$$

Considering $g_{ij}(r) = \tilde{\lambda}_{ij} \delta(r-d)$ for sticky hard-spheres when $0 < r < d$ and integrating Eq. (44) from τ to ∞ yields

$$\frac{A - A_0}{N_C kT} = - \int_{\tau}^{\infty} 12\eta_c \tilde{\lambda} \frac{d\tau'}{\tau'}, \quad (45)$$

where A_0 is the free energy of a system of hard-sphere chain with chain length m , and $\eta_c = \eta/m = \pi\rho_C d^3/6$.

The pressure Pv_0/kT of the diblock copolymer can be obtained by differentiating Eq. (45) with respect to η_c ,

$$\frac{Pv_0}{kT} - \frac{P_0v_0}{kT} = -12\eta_c^2 \int_{\tau}^{\infty} \left(\eta \frac{\partial \tilde{\lambda}}{\partial \eta} + \tilde{\lambda} \right) \frac{d\tau'}{\tau'}, \quad (46)$$

where P_0 represents the pressure of the hard sphere chains and $v_0 = \pi d^3/6$.

$$\begin{aligned} -\beta U_N(r^N) &= \sum_{a=1}^N \sum_{b>1}^N -\beta U_{ab}(|r_a - r_b|) \\ &= \sum_{i=1}^m \sum_{j=1}^m -\beta U_{ij}(|r_i - r_j|) \frac{N_i(N_j - \delta_{ij})}{2} \end{aligned} \quad (40)$$

and

$$\rho_i \rho_j g_{ij}(r_i, r_j) = \frac{1}{Z} \frac{N_i(N_j - \delta_{ij})}{2} \int e^{-\beta U_N(r_1, r_2, \dots, r_N)} dr^{N-2} \quad (41)$$

where a and b denote particles, i and j denote species.

Substituting Eq. (40) and (41) into Eq. (39) and simplifying the integral results in

$$\frac{\partial(\beta A)}{\partial \tau} = 2\pi N_C \rho_C \sum_i \sum_j \int_0^{\infty} \frac{\partial[\beta U_{ij}(r)]}{\partial \tau} g_{ij}(r) r^2 dr, \quad (42)$$

where N_C is the number of chains in the system and $\rho_i = \rho_j = \rho_C$

Note that

The quantities of hard sphere chains A_0 and P_0 can be obtained from the statistical associating fluid theory (SAFT) [42],

$$\frac{P_0}{\rho_C kT} = 1 + \frac{m(4\eta - 2\eta^2)}{(1-\eta)^3} + \frac{(1-m)(2.5\eta - \eta^2)}{(1-\eta)(1-0.5\eta)},$$

$$\begin{aligned} \frac{A_0}{N_C kT} &= \ln \eta_c + \frac{m(4\eta - 3\eta^2)}{(1-\eta)^2} + (m-1) \ln \frac{(1-\eta)^3}{(1-0.5\eta)} \\ &+ \text{terms independent of } \eta. \end{aligned} \quad (47)$$

A typical plot for the pressure of a symmetric diblock tetramer is shown in Fig. 10. The pressure increases faster at higher temperatures and approaches to the pressure of hard sphere chain fluids when $\tau \rightarrow \infty$. Van der Waals loop is not observed within the temperature range that we can explore here. Lower temperature regimes are inaccessible in this study because we are unable to solve the simultaneous transcendental equations that arises from the continuity condition of $\tilde{y}_{\alpha\beta}^{ij}(1)$ at $r=1$.

VI. CONCLUSIONS

In this paper we obtain a general solution to the multidensity Ornstein-Zernike equation in the polymer Percus-Yevick and ideal chain approximations for a primitive model of diblock hard sphere-sticky hard sphere chains. Important parameters include the attractive strength of sticky hard spheres

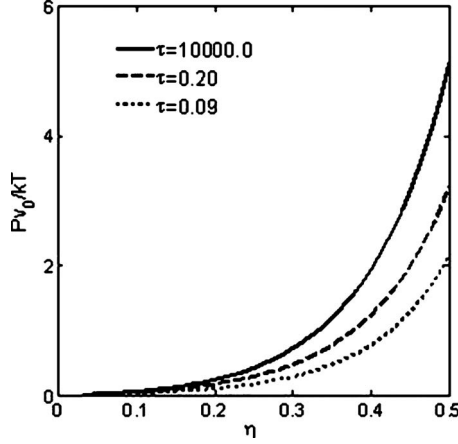


FIG. 10. Isotherms of a symmetric diblock tetramer obtained from the energy route. The quantity $v_0 = \pi d^3/6$.

τ , volume fraction of segments η , and the block lengths of both hard spheres m_h and sticky hard spheres m_s . General expressions for the contact values of the correlation functions are presented. The partial and overall radial distribution functions in the regions beyond hard core are numerically calculated from a set of integral equations using Perram's algorithm. We also investigate the static structure factors in the low and wide angle regimes. We find that low angle peaks can emerge for heteronuclear chains indicating the formation of microscopic structure. The microdomain formation is the result of a delicate balance between short range repulsive and attractive interactions within the same polymeric chain. The appearance and location of the peak (i.e., the spacing between aggregates) depends on the attractive strength, density, total chain length, and the architecture of the chains. The equation of state is also calculated via the energy route that the authors developed before. Unlike the systems of SHS dimers and chains, van der Waals loop is not observed for the heteronuclear HS-SHS diblock chains within the temperature range that we have explored. To the best of our knowledge, this is the first time the multidensity Ornstein-Zernike integral equation has been utilized to model microscopic phase formation and separation.

APPENDIX

The coefficients of the q functions in Eqs. (25) and (26) are given below,

If $i \in \{1, 2, \dots, m_h\}$,

$$\tilde{a}_0^i = \frac{2\eta + 1}{(1 - \eta)^2}, \quad \tilde{b}_0^\alpha = -\frac{3\eta}{2(1 - \eta)^2}, \quad (\text{A1a})$$

$$\tilde{a}_A^i = -\frac{\tilde{K}_i}{1 - \eta}, \quad \tilde{b}_A^i = -\frac{1}{2}\tilde{a}_A^i, \quad (\text{A1b})$$

$$\tilde{a}_B^i = -\frac{\tilde{L}_i}{1 - \eta}, \quad \tilde{b}_B^i = -\frac{1}{2}\tilde{a}_B^i. \quad (\text{A1c})$$

If $i \in \{m_h + 1, m_h + 2, \dots, m\}$,

$$\tilde{a}_0^i = \frac{2\eta + 1}{(1 - \eta)^2} - \frac{2\tilde{A}_i}{1 - \eta}, \quad \tilde{b}_0^\alpha = -\frac{3\eta}{2(1 - \eta)^2} + \frac{\tilde{A}_i}{1 - \eta}, \quad (\text{A2a})$$

$$\tilde{a}_A^i = -\frac{\tilde{K}_i + \tilde{C}_i}{1 - \eta}, \quad \tilde{b}_A^i = -\frac{1}{2}\tilde{a}_A^i, \quad (\text{A2b})$$

$$\tilde{a}_B^i = -\frac{\tilde{L}_i + \tilde{D}_i}{1 - \eta}, \quad \tilde{b}_B^i = -\frac{1}{2}\tilde{a}_B^i, \quad (\text{A2c})$$

$$\tilde{A}_i = \frac{6\eta}{m} \sum_{k=m_{h+1}}^m (\tilde{\lambda}_{00}^{ik} + \tilde{\lambda}_{0A}^{ik} + \tilde{\lambda}_{0B}^{ik}), \quad (\text{A2d})$$

$$\tilde{C}_i = \frac{12\eta}{m} \sum_{k=m_{h+1}}^m (\tilde{\lambda}_{A0}^{ik} + \tilde{\lambda}_{AA}^{ik} + \tilde{\lambda}_{AB}^{ik}), \quad (\text{A2e})$$

$$\tilde{D}_i = \frac{12\eta}{m} \sum_{k=m_{h+1}}^m (\tilde{\lambda}_{B0}^{ik} + \tilde{\lambda}_{BA}^{ik} + \tilde{\lambda}_{BB}^{ik}). \quad (\text{A2f})$$

For any i

$$\tilde{K}_i = \frac{12\eta}{m} \tilde{B}_{AB}^{i,i+1} = \frac{1}{2}(1 - \delta_{i,m}), \quad (\text{A3a})$$

$$\tilde{L}_i = \frac{12\eta}{m} \tilde{B}_{BA}^{i,i-1} = \frac{1}{2}(1 - \delta_{i,1}). \quad (\text{A3b})$$

It is not surprising that Eq. (A1) and (A2) are identical to the q functions (in functional form) of sticky hard sphere chain [23] and hard sphere chain [5,17], respectively. However, this does not indicate our solutions of diblock copolymer model can be obtained by directly superimposing the solutions of hard sphere chain and sticky hard sphere chain. This is because one of the original terminal segment effects in hard sphere chains and sticky hard sphere chains disappear in the new model of diblock copolymer. For example, the original effects of terminal bead 4 in a hard sphere tetramer and terminal bead 1 in a sticky hard sphere tetramer disappear when a new diblock octamer is composed of these two tetramers since both bead 4 and bead 1 in the original tetramers becomes inner segment 4 and 5 in the new octamer. It is also not surprising that the values of \tilde{K}_i and \tilde{L}_i are the same as those in hard sphere chains since both of them only account for the association to form chain molecules. It should be noted that \tilde{K}_i and \tilde{L}_i are independent of density in the complete association limit within the ideal chain approximation.

The explicit expressions for the contact value of correlation function $\tilde{g}_{\alpha\beta}^{ij}(1^+)$ can be evaluated from Eq. (22):

if both $\forall i \in \{1, 2, \dots, m_h\}$ and $\forall j \in \{1, 2, \dots, m_h\}$,

$$\tilde{g}_{00}^{ij}(1^+) = \frac{\eta + 2}{2(1 - \eta)^2} \quad (\text{A4a})$$

$$\tilde{g}_{A0}^{ij}(1^+) = -\frac{1}{4(1 - \eta)}(1 - \delta_{i,m}) \quad (\text{A4b})$$

$$\tilde{g}_{B0}^{ij}(1^+) = -\frac{1}{4(1-\eta)}(1-\delta_{i,1}) \quad (\text{A4c})$$

$$\tilde{g}_{AA}^{ij}(1^+) = \tilde{g}_{BB}^{ij}(1^+) = 0 \quad (\text{A4d})$$

$$\tilde{g}_{AB}^{ij}(1^+) = \frac{m}{48\eta}\delta_{j,i+2}; \quad (\text{A4e})$$

if $i \in \{m_h+1, m_h+2, \dots, m\}$ and $j \in \{1, 2, \dots, m_h\}$,

$$\tilde{g}_{00}^{ij}(1^+) = \frac{\eta+2}{2(1-\eta)^2} - \frac{6\eta}{m(1-\eta)} \sum_{k=m_h+1}^m (\tilde{\lambda}_{00}^{ik} + \tilde{\lambda}_{0A}^{ik} + \tilde{\lambda}_{0B}^{ik}), \quad (\text{A5a})$$

$$\begin{aligned} \tilde{g}_{A0}^{ij}(1^+) = & -\frac{1}{4(1-\eta)}(1-\delta_{i,m}) \\ & - \frac{6\eta}{m(1-\eta)} \sum_{k=m_h+1}^m (\tilde{\lambda}_{A0}^{ik} + \tilde{\lambda}_{AA}^{ik} + \tilde{\lambda}_{AB}^{ik}), \end{aligned} \quad (\text{A5b})$$

$$\begin{aligned} \tilde{g}_{B0}^{ij}(1^+) = & -\frac{1}{4(1-\eta)}(1-\delta_{i,1}) \\ & - \frac{6\eta}{m(1-\eta)} \sum_{k=m_h+1}^m (\tilde{\lambda}_{B0}^{ik} + \tilde{\lambda}_{BA}^{ik} + \tilde{\lambda}_{BB}^{ik}), \end{aligned} \quad (\text{A5c})$$

$$\tilde{g}_{0A}^{ij}(1^+) = -\frac{1}{4(1-\eta)}(1-\delta_{j,m}) + \frac{1}{2}(\tilde{\lambda}_{00}^{i,j+1} + \tilde{\lambda}_{0A}^{i,j+1})\delta_{j,m_h}, \quad (\text{A5d})$$

$$\tilde{g}_{0B}^{ij}(1^+) = -\frac{1}{4(1-\eta)}(1-\delta_{j,1}), \quad (\text{A5e})$$

$$\tilde{g}_{AA}^{ij}(1^+) = \frac{1}{2}(\tilde{\lambda}_{A0}^{i,j+1} + \tilde{\lambda}_{AA}^{i,j+1})\delta_{j,m_h}, \quad (\text{A5f})$$

$$\tilde{g}_{BB}^{ij}(1^+) = 0, \quad (\text{A5g})$$

$$\tilde{g}_{AB}^{ij}(1^+) = 0, \quad (\text{A5h})$$

$$\begin{aligned} \tilde{g}_{BA}^{ij}(1^+) = & \frac{m}{48\eta}\delta_{j,i-2}(1-\delta_{j,m_h}) \\ & + \frac{1}{2}(\tilde{\lambda}_{B0}^{i,m_h+1} + \tilde{\lambda}_{BA}^{i,m_h+1})\delta_{j,m_h} + \frac{m}{48\eta}\delta_{j,m_h}\delta_{i,m_h+2}. \end{aligned} \quad (\text{A5i})$$

If $i \in \{m_h+1, m_h+2, \dots, m\}$ and $j \in \{m_h+1, m_h+2, \dots, m_h\}$,

$$\tilde{g}_{00}^{ij}(1^+) = 12\tau\tilde{\lambda}_{00}^{ij} = \frac{\eta+2}{2(1-\eta)^2} - \frac{\tilde{A}_i}{1-\eta} + \frac{12\eta}{m} \sum_{k=m_h+1}^m \left[\left(-\frac{1}{2(1-\eta)} + \tilde{\lambda}_{00}^{ik} \right) (\tilde{\lambda}_{00}^{kj} + \tilde{\lambda}_{A0}^{kj} + \tilde{\lambda}_{B0}^{kj}) + \tilde{\lambda}_{0A}^{ik}(\tilde{\lambda}_{00}^{kj} + \tilde{\lambda}_{B0}^{kj}) + \tilde{\lambda}_{0B}^{ik}(\tilde{\lambda}_{00}^{kj} + \tilde{\lambda}_{A0}^{kj}) \right], \quad (\text{A6a})$$

$$\tilde{g}_{A0}^{ij}(1^+) = 12\tau\tilde{\lambda}_{A0}^{ij} = -\frac{\tilde{K}_i + \tilde{C}_i}{2(1-\eta)} + \frac{12\eta}{m} \sum_{k=m_h+1}^m [\lambda_{A0}^{ik}(\tilde{\lambda}_{00}^{kj} + \tilde{\lambda}_{A0}^{kj} + \tilde{\lambda}_{B0}^{kj}) + \tilde{\lambda}_{AA}^{ik}(\tilde{\lambda}_{00}^{kj} + \tilde{\lambda}_{B0}^{kj}) + \tilde{\lambda}_{AB}^{ik}(\tilde{\lambda}_{00}^{kj} + \tilde{\lambda}_{A0}^{kj})] + \frac{1}{2}(\tilde{\lambda}_{00}^{i+1,j} + \tilde{\lambda}_{A0}^{i+1,j}), \quad (\text{A6b})$$

$$\tilde{g}_{B0}^{ij}(1^+) = 12\tau\tilde{\lambda}_{B0}^{ij} = -\frac{\tilde{L}_i + \tilde{D}_i}{2(1-\eta)} + \frac{12\eta}{m} \sum_{k=m_h+1}^m [\lambda_{B0}^{ik}(\tilde{\lambda}_{00}^{kj} + \tilde{\lambda}_{A0}^{kj} + \tilde{\lambda}_{B0}^{kj}) + \tilde{\lambda}_{BA}^{ik}(\tilde{\lambda}_{00}^{kj} + \tilde{\lambda}_{B0}^{kj}) + \tilde{\lambda}_{BB}^{ik}(\tilde{\lambda}_{00}^{kj} + \tilde{\lambda}_{A0}^{kj})] + \frac{1}{2}(\tilde{\lambda}_{00}^{i-1,j} + \tilde{\lambda}_{B0}^{i-1,j}), \quad (\text{A6c})$$

$$\tilde{g}_{AA}^{ij}(1^+) = 12\tau\tilde{\lambda}_{AA}^{ij} = \frac{12\eta}{m} \sum_{k=m_h+1}^m [\tilde{\lambda}_{A0}^{ik}(\tilde{\lambda}_{0A}^{kj} + \tilde{\lambda}_{AA}^{kj} + \tilde{\lambda}_{BA}^{kj}) + \tilde{\lambda}_{AA}^{ik}(\tilde{\lambda}_{0A}^{kj} + \tilde{\lambda}_{BA}^{kj}) + \tilde{\lambda}_{AB}^{ik}(\tilde{\lambda}_{0A}^{kj} + \tilde{\lambda}_{AA}^{kj})] + \frac{1}{2}(\tilde{\lambda}_{A0}^{i,j+1} + \tilde{\lambda}_{AA}^{i,j+1}) + \frac{1}{2}(\tilde{\lambda}_{0A}^{i+1,j} + \tilde{\lambda}_{AA}^{i+1,j}), \quad (\text{A6d})$$

$$\tilde{g}_{BB}^{ij}(1^+) = 12\tau\tilde{\lambda}_{BB}^{ij} = \frac{12\eta}{m} \sum_{k=m_h+1}^m [\lambda_{B0}^{ik}(\tilde{\lambda}_{0B}^{kj} + \tilde{\lambda}_{AB}^{kj} + \tilde{\lambda}_{BB}^{kj}) + \tilde{\lambda}_{BA}^{ik}(\tilde{\lambda}_{0B}^{kj} + \tilde{\lambda}_{BB}^{kj}) + \tilde{\lambda}_{BB}^{ik}(\tilde{\lambda}_{0B}^{kj} + \tilde{\lambda}_{AB}^{kj})] + \frac{1}{2}(\tilde{\lambda}_{B0}^{i,j-1} + \tilde{\lambda}_{BB}^{i,j-1}) + \frac{1}{2}(\tilde{\lambda}_{0B}^{i-1,j} + \tilde{\lambda}_{BB}^{i-1,j}), \quad (\text{A6e})$$

$$\begin{aligned} \tilde{g}_{AB}^{ij}(1^+) = 12\tau\tilde{\lambda}_{AB}^{ij} = \frac{12\eta}{m} \sum_{k=m_h+1}^m [\lambda_{A0}^{ik}(\tilde{\lambda}_{0B}^{kj} + \tilde{\lambda}_{AB}^{kj} + \tilde{\lambda}_B^{kj}) + \tilde{\lambda}_{AA}^{ik}(\tilde{\lambda}_{0B}^{kj} + \tilde{\lambda}_{BB}^{kj}) + \tilde{\lambda}_{AB}^{ik}(\tilde{\lambda}_{0B}^{kj} + \tilde{\lambda}_{AB}^{kj})] \\ + \frac{1}{2}(\tilde{\lambda}_{A0}^{i,j-1} + \tilde{\lambda}_{AB}^{i,j-1}) + \frac{1}{2}(\tilde{\lambda}_{0B}^{i+1,j} + \tilde{\lambda}_{AB}^{i+1,j}) + \frac{m}{48\eta}\delta_{j,i+2}, \end{aligned} \quad (\text{A6f})$$

By symmetry, it is clear that $\tilde{\lambda}_{\alpha\beta}^{ij} = \tilde{\lambda}_{\beta\alpha}^{ji}$ for $i \in \{m_h+1, m_h+2, \dots, m\}$ and $j \in \{m_h+1, m_h+2, \dots, m\}$, and $\tilde{g}_{\alpha\beta}^{ij}(1^+) = \tilde{g}_{\beta\alpha}^{ji}(1^+)$ for any pair of ij .

-
- [1] M. S. Wertheim, *J. Stat. Phys.* **35**, 19 (1984).
[2] M. S. Wertheim, *J. Stat. Phys.* **35**, 35 (1984).
[3] M. S. Wertheim, *J. Stat. Phys.* **42**, 459 (1986).
[4] M. S. Wertheim, *J. Stat. Phys.* **42**, 477 (1986).
[5] J. Chang and S. I. Sandler, *J. Chem. Phys.* **102**, 437 (1995); **103**, 3196 (1995).
[6] M. S. Yeom, J. Chang, and H. Kim, *J. Korean Phys. Soc.* **47**, 822 (2005).
[7] M. S. Wertheim, *J. Chem. Phys.* **85**, 2929 (1986).
[8] A. O. Weist and E. D. Glandt, *J. Chem. Phys.* **97**, 4316 (1992).
[9] Y. V. Kalyuzhnyi, I. A. Protsykevych, and M. F. Holovko, *Chem. Phys. Lett.* **215**, 1 (1993).
[10] Y. V. Kalyuzhnyi, L. Blum, J. Rescic, and G. Stell, *J. Chem. Phys.* **113**, 1135 (2000).
[11] N. von Solms and Y. C. Chiew, *J. Chem. Phys.* **113**, 6316 (2000).
[12] N. von Solms and Y. C. Chiew, *J. Chem. Phys.* **111**, 4839 (1999); *J. Stat. Phys.* **100**, 267 (2000).
[13] N. von Solms and Y. C. Chiew, *J. Chem. Phys.* **118**, 4321 (2003).
[14] N. Wu and Y. C. Chiew, *J. Chem. Phys.* **115**, 6641 (2001).
[15] Y. V. Kalyuzhnyi and P. T. Cummings, *J. Chem. Phys.* **103**, 3265 (1995).
[16] J. Chang and H. Kim, *J. Chem. Phys.* **109**, 2579 (1998).
[17] Y. V. Kalyuzhnyi, C. T. Lin, and G. Stell, *J. Chem. Phys.* **106**, 1940 (1997).
[18] G. Stell, C. T. Lin, and Y. V. Kalyuzhnyi, *J. Chem. Phys.* **110**, 5444 (1999); **110**, 5458 (1999).
[19] C. T. Lin, G. Stell, and Y. V. Kalyuzhnyi, *J. Chem. Phys.* **112**, 3071 (2000).
[20] Y. V. Kalyuzhnyi, C. McCabe, P. T. Cummings, and G. Stell, *Mol. Phys.* **100**, 2499 (2002).
[21] C. McCabe, Y. V. Kalyuzhnyi, and P. T. Cummings, *Fluid Phase Equilib.* **194–197**, 185 (2002).
[22] N. Wu, S. S. Feng, and Y. C. Chiew, *J. Chem. Phys.* **117**, 4462 (2002).
[23] N. Wu, S. S. Feng, and Y. C. Chiew, *J. Chem. Phys.* **118**, 10794 (2003).
[24] S. Granick, S. Jiang, and Q. Chen, *Phys. Today* **62** (7), 68 (2009).
[25] Z. L. Zhang and S. C. Glotzer, *Nano Lett.* **4**, 1407 (2004).
[26] J. W. Kim, R. J. Larsen, and D. A. Weitz, *J. Am. Chem. Soc.* **128**, 14374 (2006).
[27] J. G. Park, J. D. Forster, and E. R. Dufresne, *Langmuir* **25**, 8903 (2009).
[28] G. A. DeVries, M. Brunnbauer, Y. Hu, A. M. Jackson, B. Long, B. Neltner, O. Uzun, B. H. Wunsch, and F. Stellacci, *Science* **315**, 358 (2007).
[29] E. Bianchi, J. Largo, P. Tartaglia, E. Zaccarelli, and F. Sciortino, *Phys. Rev. Lett.* **97**, 168301 (2006).
[30] F. Sciortino, A. Giacometti, and G. Pastore, *Phys. Rev. Lett.* **103**, 237801 (2009).
[31] R. J. Baxter, in *Physical Chemistry: An Advanced Treatise, Vol. VIII A*, edited by H. Eyring, D. Henderson, and W. Jost (Academic, New York, 1971).
[32] M. P. Tosi, *J. Phys. Condens. Matter* **6**, A13 (1994).
[33] D. Gazzillo, R. Fantoni, and A. Giacometti, *Mol. Phys.* **104**, 3451 (2006); D. Gazzillo, A. Giacometti, R. Fantoni, and P. Sollich, *Phys. Rev. E* **74**, 051407 (2006); R. Fantoni, D. Gazzillo, and A. Giacometti, *J. Chem. Phys.* **122**, 034901 (2005).
[34] S. V. G. Menon, V. K. Kelkar, and C. Manohar, *Phys. Rev. A* **43**, 1130 (1991).
[35] S. H. Chen, J. Rouch, F. Sciortino, and P. Tartaglia, *J. Phys.: Condens. Matter* **6**, 10855 (1994).
[36] Y. C. Chiew, *J. Chem. Phys.* **110**, 10482 (1999); Y. C. Chiew and E. D. Glandt, *J. Phys. A* **16**, 2599 (1983); **22**, 3969 (1989).
[37] E. Dickinson, *J. Chem. Soc., Faraday Trans.* **93**, 2297 (1997).
[38] R. Piazza, V. Peyre, and V. Degiorgio, *Phys. Rev. E* **58**, R2733 (1998).
[39] S. Ramakrishnan and C. F. Zukoski, *J. Chem. Phys.* **113**, 1237 (2000).
[40] Y. V. Kalyuzhnyi, C. T. Lin, and G. Stell, *J. Chem. Phys.* **108**, 6525 (1998).
[41] J. W. Perram, *Mol. Phys.* **30**, 1505 (1975).
[42] S. H. Huang and M. Radosz, *Ind. Eng. Chem. Res.* **29**, 2284 (1990); S.-j. Chen, Y. C. Chiew, J. A. Gardecki, S. Nilsen, and M. Radosz, *J. Polym. Sci., Part B: Polym. Phys.* **32**, 1791 (1994).